6. D. M. Eardley *et al.*, *Phys. Rev. Lett.* **30**, 884 (1973); D. M. Eardley, D. L. Lee, A. P. Lightman, *Phys. Rev. D* **8**, 3308 (1973).
7. K. S. Thorne, in *Gravitational Radiation*, N. Deruelle and T. Piran, Eds. (North-Holland, Dordrecht, Netherlands, 1983), pp. 1–54.
8. L. S. Finn, A. Ori, K. S. Thorne, in preparation.
9. S. L. Detweiler, *Astrophys. J.* **225**, 687 (1978); ______ and E. Szedenits, *ibid.* **231**, 211 (1979); T. Nakamura, K. Oohara, Y. Kojima, *Prog. Theor. Phys.* (*suppl.*) **90**, 1 (1987).
10. See, for example, C. R. Evans, L. S. Finn, D. W. Hobill, Eds., *Frontiers in Numerical Relativity* (Cambridge Univ. Press, Cambridge, 1989); G. B. Cook and J. W. York, *Phys. Rev. D* **41**, 1077 (1989); J. Bowen, J. Rauber, J. W. York, *Class. Quantum Gravity* **1**, 591 (1984); L. Smarr, *Ann. N.Y. Acad. Sci.* **301**, 569 (1977).
11. See, for example, S. L. Shapiro and S. A. Teukolsky, *Black Holes, White Dwarfs, and Neutron Stars* (Wiley, New York, 1983).
12. For the history of radio astronomy and the revolution it brought, see K. Kellermann and B. Sheets, Eds., *Serendipitous Discoveries in Radio Astronomy* (National Radio Astronomy Observatory, Green Bank, WV, 1983); W. T. Sullivan, Ed., *Classics in Radio Astronomy* (Kluwer, Dordrecht, Netherlands, 1982); *The Early Years of Radio Astronomy* (Cambridge Univ. Press, Cambridge, 1984).
13. K. S. Thorne, in *300 Years of Gravitation*, S. W. Hawking and W. Israel, Eds. (Cambridge Univ. Press, Cambridge, 1987), pp. 330–458.
14. For discussions and lists of references, see (*13*) and K. S. Thorne, in *Recent Advances in General Relativity*, A. Janis and J. Porter, Eds. (Birkhauser, Boston, 1992), pp. 196–229.
15. D. G. Blair, Ed., *The Detection of Gravitational Waves* (Cambridge Univ. Press, Cambridge, 1991).
16. Bar detectors were invented by J. Weber [*Phys. Rev.* **117**, 306 (1960)] and have been developed to a high degree of sophistication since then; see, for example, P. F. Michelson, J. C. Price, R. C. Taber, *Science* **237**, 150 (1987); (*15*).
17. The seeds of the idea for laser interferometer gravitational-wave detectors are contained in F. A. E. Pirani, *Acta Phys. Pol.* **15**, 389 (1956), in M. E. Gertsenshtein and V. I. Pustovoit, *Sov. Phys. JETP* **16**, 433 (1963), and in J. Weber's personal notebooks from the 1960s; the first detailed descriptions of the idea were by G. E. Moss, L. R. Miller, and R. L. Forward [*Appl. Opt.* **10**, 2495 (1971)] and by R. Weiss [*Quart. Prog. Rep. Res. Lab. Electron. M.I.T.* **105**, 54 (1972)].
18. R. W. P. Drever, in *Gravitational Radiation*, N. Deruelle and T. Piran, Eds. (North-Holland, Dordrecht, Netherlands, 1983), pp. 321–338; R. W. P. Drever *et al.*, in *Quantum Optics, Experimental Gravity, and Measurement Theory*, P. Meystre and M. O. Scully, Eds. (Plenum, New York, 1983), pp. 503–514, and references therein.
19. For example, the two arms can be operated as optical delay lines, with the bouncing light in them making many discrete spots on the mirrors instead of being trapped in a Fabry-Perot cavity [R. Weiss, in (*17*)]. This configuration is now being developed in Europe (*15*).
20. B. J. Meers, *Phys. Rev. D* **38**, 2317 (1988); K. A. Strain and B. J. Meers, *Phys. Rev. Lett.* **66**, 1391 (1991); and references therein.
21. The many laser beams in each arm may include (i) up to six simultaneous Fabry-Perot cavity beams after an upgrade of LIGO's corner and end stations, (ii) beams connecting the suspension points of the test masses (*27*) as part of seismic isolation systems (see Fig. 5 for an example); and (iii) the many individual beams of a single interferometer with arms that are optical delay lines rather than Fabry-Perot cavities (*19*).
22. Some noise sources will be common to the vacuum-sharing 4- and 2-km interferometers. However, many will not be common, and those that are will typically not mimic a true gravitational wave's 2:1 ratio of signal strengths.
23. Y. Gürsel and M. Tinto, *Phys. Rev. D* **40**, 3884 (1990).
24. Similarly, when used in the study of periodic waves (such as from a pulsar) with amplitude h_{amp} and frequency f, the interferometer will have the signal-to-noise ratio (*13*)
$$\frac{S}{N}=\frac{h_{\mathrm{amp}}\sqrt{\tau_{\mathrm{int}}}}{\tilde{h}(f)}$$
where τ_{int} is the total time over which the periodic signal is integrated.
25. P. Fritschel, D. Shoemaker, R. Weiss, *Appl. Opt.*, in press.
26. R. L. Rinker and J. E. Faller, in "Precision instruments and fundamental constants II," B. N. Taylor and W. D. Phillips, Eds., *National Bureau of Standards Spec. Pub.* **617**, 411 (1984); N. A. Robertson *et al.*, *J. Phys. E* **15**, 1101 (1982); P. R. Saulson, *Rev. Sci. Instrum.* **15**, 1315 (1984); N. A. Robertson, in *The Detection of Gravitational Waves*, D. Blair, Ed. (Cambridge Univ. Press, Cambridge, 1990), pp. 353–368.
27. R. W. P. Drever, in *The Detection of Gravitational Waves*, D. Blair, Ed. (Cambridge Univ. Press, Cambridge, 1990), pp. 306–328.
28. A technical description of the prototype and experiments that have been carried out with it will be published soon.
29. R. W. P. Drever *et al.*, *Appl. Phys.* **B31**, 97 (1983).
30. B. F. Schutz, *Nature* **323**, 310 (1986); *Class. Quantum Gravity* **6**, 1761 (1989); H. D. Wahlquist, *Gen. Relativ. Gravit.* **19**, 1101 (1987).
31. C. W. Lincoln and C. M. Will, *Phys. Rev. D* **42**, 1123 (1990).
32. E. S. Phinney, *Astrophys. J.* **380**, L17 (1991).
33. R. Narayan *et al.*, *ibid.* **379**, L17 (1991).
34. From equation 46b of (*7*), with a $\sqrt{2}$ correction added because of the incorrect use of ft rather than $\int(df/dt)dt$ in equation 42 of (*7*), and with neutron star masses of 1.4 solar masses.
35. Because the burst is far out on the tail of the noise's Gaussian probability distribution, h_{SB} is quite insensitive to whether the time between bursts is 1 month or 1 year and to whether by "highly confident" one means 90% or 99%. The factor 11 in Eq. 9 is made up of (i) a factor of $\sqrt{5}$ that is included because, owing to the detectors' quadrupolar beam pattern, waves from a random (typical) direction produce a signal $\sqrt{5}$ times as small as that from an optimal direction and (ii) a factor of 5 from the Gaussian statistics for two identical 4-km interferometers that search for events of duration ~0.01 s that occur a few times per year. See (*13*) for a more careful analysis and discussion; in that reference h_{SB} is called $h_{3/\mathrm{yr}}$.
36. P. Haensel, B. Paczynski, P. Amsterdamski, *Astrophys. J.* **375**, 209 (1991).
37. See, for example, S. E. Woosley and T. A. Weaver, *Annu. Rev. Astron. Astrophys.* **24**, 205 (1986).
38. R. Mönchmeyer, G. Schäfer, E. Müller, R. E. Kates, *Astron. Astrophys.* **246**, 417 (1991); L. S. Finn, *Ann. N.Y. Acad. Sci.* **631**, 156 (1991).
39. See, for example, the following references for discussion of this so-called "bar mode instability" in various contexts: S. Chandrasekhar, *Ellipsoidal Figures of Equilibrium* (Yale Univ. Press, New Haven, CT, 1969); J. R. Ipser and L. Lindblom, *Phys. Rev. Lett.* **62**, 2777 (1989); *Astrophys. J.* **355**, 226 (1990).
40. For the rates of supernova explosions, see S. van den Bergh and G. A. Tammann, *Annu. Rev. Astron. Astrophys.* **29**, 363 (1991).
41. This wave strength h_c is independent of the strength of the instability and the resulting degree of nonaxisymmetry as long as the gravitational waves are responsible for carrying away the core's angular momentum. For weaker instabilities, the waves' amplitude h_{amp} is smaller and the number of cycles n that the waves spend near a frequency f is larger; the product $h_c \simeq h_{\mathrm{amp}}\sqrt{n}$ is constant.
42. D. A. Frail and S. R. Kulkarni, *Nature* **352**, 785 (1991).

43. This work was supported in part by NSF grant PHY-8803557.

Global Tectonics and Space Geodesy

Richard G. Gordon and Seth Stein

Much of the success of plate tectonics can be attributed to the near rigidity of tectonic plates and the availability of data that describe the rates and directions of motion across narrow plate boundaries ~1 to 60 kilometers wide. Nonetheless, many plate boundaries in both continental and oceanic lithosphere are not narrow but are hundreds to thousands of kilometers wide. Wide plate boundary zones cover ~15 percent of Earth's surface area. Space geodesy, which includes very long baseline radio interferometry, satellite laser ranging, and the global positioning system, is providing the accurate long-distance measurements needed to estimate the present motion across and within wide plate boundary zones. Space geodetic data show that plate velocities averaged over years are remarkably similar to velocities averaged over millions of years.

Plate motion, Earth's most important tectonic process, was first quantitatively described about 25 years ago (*1*, *2*). Earth's strong outer layer that composes the plates is termed the lithosphere, which typically comprises the crust plus the uppermost mantle and is of variable thickness but may typically be ~100 km thick. The presumably much weaker layer immediately below the lithosphere is termed the asthenosphere. Plate tectonics is the culmination of the hypothesis of seafloor spreading (*3*). That geomagnetic reversals are recorded by the seafloor as it spreads away from mid-ocean ridges (*4*) made possible the confirmation of seafloor spreading and the estimation of seafloor spreading rates (*5*).

The authors are in the Department of Geological Sciences, Northwestern University, Evanston, IL 60208.

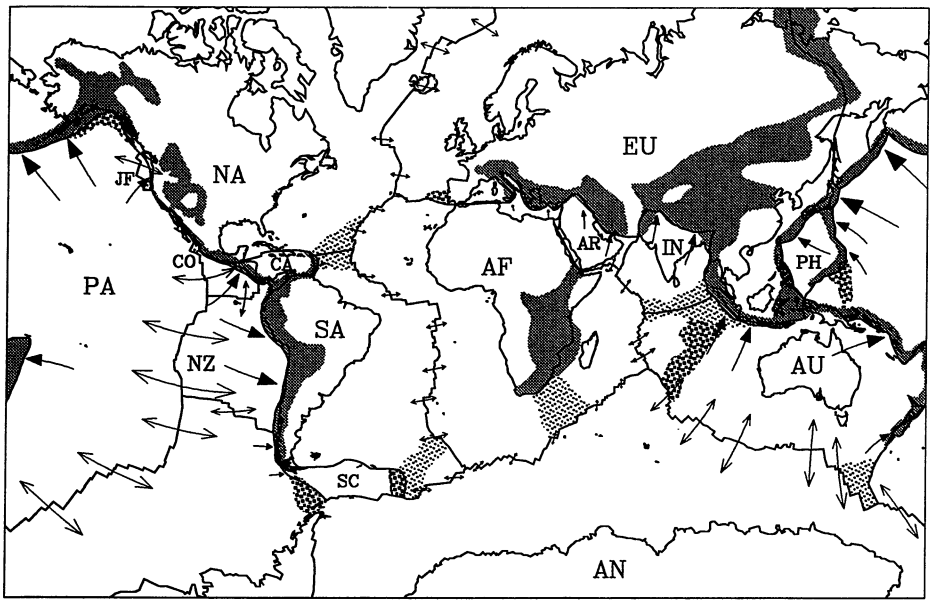

Fig. 1. Map showing idealized narrow plate boundaries, velocities between plates, and regions of deforming lithosphere (*81*). Plate velocities are shown by arrows. The length of the arrows shows what the displacement would be if the plates were to maintain their present relative angular velocity for 25 million years. The plate separation rate across mid-ocean ridges is shown by symmetrical diverging arrows with unclosed arrowheads at both ends. The plate convergence rate is shown by asymmetrical arrows with one solid arrowhead, which are shown on the underthrust plate where convergence is asymmetric and the polarity is known. Each convergence arrow points toward the overthrust plate. The outlines of deforming regions are approximate and the existence of some deforming zones is speculative. Fine stipple shows mainly subaerial regions where the deformation has been inferred from seismicity, topography, other evidence of faulting, or some combination of these. Medium stipple shows mainly submarine regions where the nonclosure of plate circuits indicates measurable deformation; in most cases these zones are also marked by earthquakes. Coarse stipple shows mainly submarine regions where the deformation is inferred mainly from the presence of earthquakes. (Compare with earthquake locations in Fig. 2.) These deforming regions form wide plate boundary zones, which cover ~15% of Earth's surface. Future observations may demonstrate that deforming lithosphere covers an area larger or smaller than shown here. Plate name abbreviations: AF, Africa; AN, Antarctica; AR, Arabia; AU, Australia; CA, Caribbean; CO, Cocos; EU, Eurasia; JF, Juan de Fuca; IN, India; NA, North America; NZ, Nazca; PA, Pacific; PH, Philippine Sea; SA, South America; SC, Scotia Sea.

Analysis of magnetic anomalies over mid-ocean ridges shows that plate separation rates over the past few million years vary from a low of 12 mm/year across the Arctic Ridge to a high of 160 mm/year across the East Pacific Rise between the Pacific and Nazca plates, with a median rate of ~40 mm/year (Fig. 1). Convergence rates between the stable interiors of plates meeting at deep sea trenches range from a low of ~20 mm/year along the southern Chile trench, where the Antarctic plate underthrusts the South American plate, to ~110 mm/year along the Australia-Pacific plate boundary, with a median rate of ~70 mm/year (6) (Fig. 1).

Because tectonic plates move along the nearly spherical surface of Earth, motion between plates can be represented simply as rigid body rotations. In the limiting case of geologically instantaneous motion (that is, the average over a few million years), the rigid body rotations can be described by angular velocity vectors. The assumption of plate rigidity allows geometrically precise and rigorously testable predictions to be made. The observed near rigidity of the plates also permits the treatment of plate kinematics separately from the dynamics. Abundant data describe the geologically instantaneous motion across the narrow boundaries that separate nearly all the major plates, permitting many tests of plate tectonic predictions.

In this article, we first review geologically instantaneous plate kinematics and discuss many observations that do not conform to plate tectonic theory. We then describe the recent success of and potential for further progress from applications of space geodesy to tectonic problems. Space geodetic data have already shown that plate velocities averaged over several years are similar to those averaged over millions of years and have helped to quantify the deformation in wide plate boundary zones. Current and planned research using space geodesy promises many advances in understanding the kinematics of plate boundary zones with implications for the forces that drive plate motion, build mountains, and cause earthquakes.

Plate Boundary Zones

A plate boundary zone is the zone of active deformation that takes up the motion between nearly rigid plates. Earth's surface would be covered completely by a mosaic of plates that interact only along their edges if plate boundaries were lines having no width (Fig. 1). Real plate boundary zones, however, vary in width from a few hundred meters (*7, 8*) for some oceanic transform fault plate boundaries to thousands of kilometers within the deforming zone taking up motion between India and Eurasia (9) (Fig. 1). Herein we refer to plate boundary zones as narrow if they are up to ~60 km wide, the maximum width of the plate boundary zones of mid-ocean ridges (*10*), and wide if they are hundreds to thousands of kilometers wide.

Plate boundaries can be classified into three types depending on whether the motion between two plates (i) contains a component of divergence, (ii) contains a component of convergence, or (iii) is parallel to the boundary with no convergence or divergence. The most common examples of the first are mid-ocean ridges where the divergence is distributed over a plate boundary zone, which can be as narrow as 8 to 20 km wide at fast spreading centers or as wide as to ~60 km at slow spreading centers. Most of the divergence, however, is presumably concentrated in the neovolcanic zone (the area straddling the spreading axis in which most of the recent and ongoing surficial volcanism occurs), which is typically 1 to 3 km wide (*10*). The most common examples of the second are deep sea trenches where oceanic lithosphere of one plate is subducted beneath another plate. A line of volcanoes on the overriding plate marks the surface arc below which the subducting plate reaches a depth of ~100 km. Permanent deformation associated with trench plate boundaries is in many regions distributed within the overriding plate for hundreds of kilometers, but most of the motion is likely taken up along a single thrust fault zone, which may be only a few kilometers or less thick. The third type of plate boundary occurs in almost every case as a submarine transform fault, which with few exceptions offsets two mid-ocean ridge segments. Transform faults are vertical faults along which horizontal slip occurs parallel to the direction of relative plate motion. Continental transform faults are rarer and much further from the geometrical ideal than are submarine faults. Seafloor-imaging studies using multi-beam and side-scan sonar show that the active trace of submarine transform faults, which is termed the transform fault zone and constitutes the plate boundary zone, is typically 0.5 to 2 km wide (7, 8).

Plate Tectonic Data

The ability to make and to test plate tectonic predictions grows with the accuracy of the available observations. For the past 25 years, our knowledge of geologically instantaneous plate motions has depended mainly upon three types of data, which we will refer to as "conventional" plate motion data. The first type consists of spreading rates estimated from the observed spacing of magnetic anomalies across mid-ocean ridges. The spacing of the magnetic anomalies can be used to estimate rates of seafloor spreading, provided that the history of geomagnetic reversals is accurately known. In the past 25 years the acquisition of marine magnetic anomaly data for determining seafloor spreading rates has not changed fundamentally. However, the number and quality of data have improved through expanded geographical coverage, more accurate navigation, and the acquisition of closely spaced profiles and of profiles paralleling the direction of plate motion. The shortest interval over which spreading rates can be determined is the interval between geomagnetic reversals, which ranges from tens of thousands to tens of millions of years (*11*). The shortest possible averaging interval for geologically instantaneous spreading rates is 780,000 years, the age of the most recent geomagnetic reversal (*12*), but rates are more typically averaged over the past few million years.

The second data type is the azimuth of a submarine transform fault estimated from bathymetric observations. Although submarine transform fault zones are narrow, they typically consist of several parallel fault strands. For the approximation to a single fault to be reasonable, the fault system should be long compared with its width. The overall azimuth of the fault zone, and not the azimuth of individual faults within it, is used to estimate the direction of relative plate motion. The accuracy with which the azimuth of transforms can be estimated depends on the type of bathymetric data used. Azimuths estimated from surveys that use precision depth recording are less accurate (about $\pm 10°$) than azimuths from multi-beam or side-scan sonar bathymetry (about $\pm 3°$) (*8, 13, 14*). The poorly known time interval over which the azimuth of a transform fault averages motion is probably less than millions of years, but more than centuries. Thus, the interval averaged by transform fault azimuths is probably shorter than that averaged by spreading rates.

The third data type is the slip direction calculated from focal mechanisms inferred from the radiation pattern of seismic waves from earthquakes along transform faults or at trenches. The slip directions from large earthquakes along submarine transform faults give less accurate ($\pm 10°$ to $\pm 15°$) estimates of plate motion direction than are obtained from fault azimuths (*13, 14*). The horizontal projection of the slip direction in shallow thrust-fault earthquakes at trenches provides the largest number of azimuths used to estimate plate motions. Because the slip in earthquakes releases the strain accumulated over decades, centuries, or millennia, earthquake slip directions probably average motion over a much shorter interval than is averaged by spreading rates or by transform fault azimuths. The quantity and the quality of estimates of earthquake slip directions have improved during the past decade. Before the 1980s, nearly all seismological data were in analog form. Most focal mechanisms were estimated only from the polarity of the first motion of body waves, with little or no use made from the information in the rest of the seismogram. Digitally recorded data, which have become widely and rapidly available over the past decade through computer and telephone networks, facilitate the routine use of waveform modeling to estimate earthquake focal

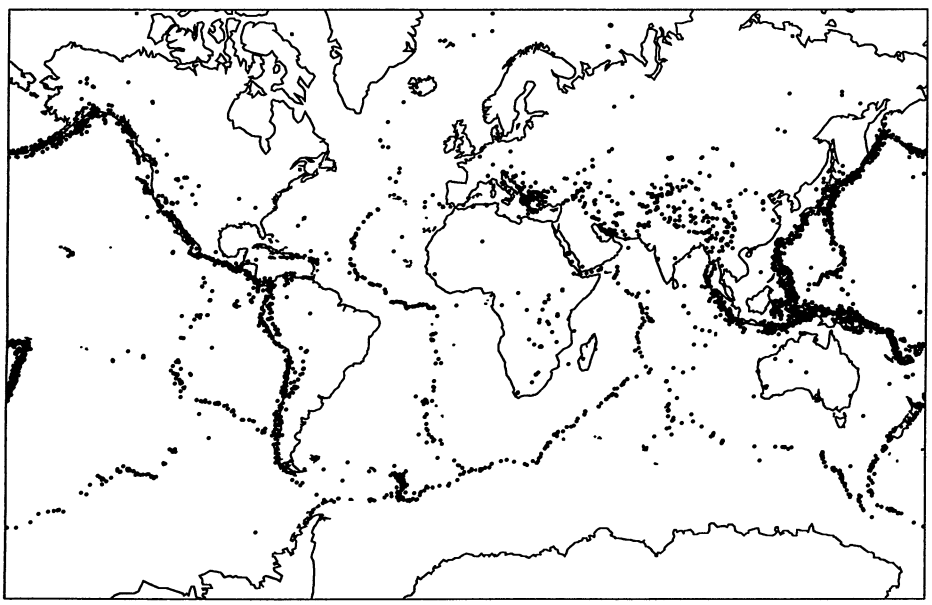

Fig. 2. Map showing all earthquakes shallower than 50 km and with magnitudes of at least 5.5 from 1963 to 1987 from the catalog of the National Earthquake Information Center. Bands of earthquakes are narrow along most oceanic plate boundaries and wide along most continental and some oceanic plate boundaries.

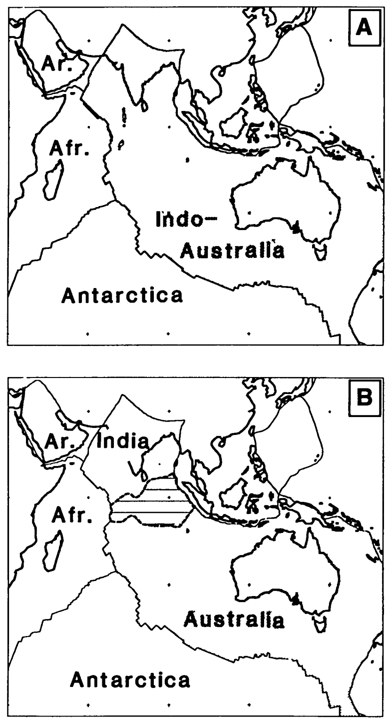

Fig. 3. Proposed plate geometries for the Indian Ocean. (**A**) The old model for the plate geometry. India and Australia lie on the same plate (the Indo-Australian plate). The Arabian plate is separated from the Indo-Australian plate along a boundary that includes the Owen fracture zone. (**B**) The geometry that is best fit by geologically instantaneous plate motion data. Australia, India, and Arabia lie on distinct plates. The Australian and Indian plates are separated by a wide plate boundary zone (region with horizontal rules), and the Arabian and Indian plates are separated by a boundary that includes the Owen fracture zone. Published with the permission of the American Geophysical Union [after (*26*)].

mechanisms.

Global models of the geologically instantaneous motion between plates are determined by systematic inversion of all available conventional plate motion data (*14–16*). Such a model is described by a set of angular velocity vectors specifying the motion of each plate relative to one arbitrarily fixed plate. The angular velocity vector describing the motion between any pair of plates can then be determined by vector subtraction. Angular velocity vectors are in many cases specified in spherical coordinates by their rotation rate (magnitude) and Euler pole (latitude and longitude). The velocity of one plate relative to another at any point along their mutual narrow plate boundary is the cross product of the appropriate angular velocity vector and the point position vector. The most recently published global plate motion model, NUVEL-1, gives a good fit to all available conventional plate motion data (*14*).

Plate Tectonic Anomalies

Early in the attempts to apply the tectonics of rigid plates to active deformation, it was recognized that plate tectonics poorly describes the kinematics and tectonics of continental plate boundary zones. Wherever plate boundaries pass through continents, the boundaries are hundreds to thousands of kilometers wide (Fig. 1). Continental crust, and possibly the lithospheric mantle beneath it, does not participate in the convection of the solid Earth because it has too low a density for more than a small volume to be subducted (*17*). Laboratory deformation studies suggest that there should be large differences between the strength profiles of continental and oceanic lithosphere (*18*). Continental crustal rheology is thought to be controlled by the properties of quartz or feldspar, whereas the rheology of the upper mantle is thought to be controlled by the properties of olivine. For a given mineralogy, rock strength is expected to increase with depth in the colder, near-surface brittle regime, and then decrease with depth below the brittle-plastic transition because the strength in the plastic regime decreases with temperature. Oceanic lithosphere is therefore expected to have a simple strength profile: strongest near mid-lithospheric depths and weakest near its top and bottom. Continental lithosphere is more complicated because continental crust likely deforms according to a quartz (or feldspar) flow law, whereas the mantle portion has a stronger olivine-controlled rheology. Laboratory experiments suggest that olivine is stronger at depth than is quartz. Consequently continental lithosphere is expected to have two maxima in strength: the greater maximum is in the uppermost mantle and the second, lesser maximum is at ~15 km depth in the crust, within the brittle-plastic transition. The weaker, lower crust lies between the two strength maxima. When continental lithosphere deforms, especially when plate motion brings two continents into collision, much of the continental crust may detach from the lithospheric mantle and pile up to form mountain ranges and broad high plateaus, as in the Himalayas and Tibetan plateau (*19*).

Less obvious has been the failure of plate tectonics to describe the kinematics of all oceanic lithosphere. The distribution of earthquake epicenters in the oceans differs considerably from that on the continents. In contrast to the wide bands of earthquakes marking continental plate boundaries, narrow bands of earthquakes no wider than a few tens of kilometers mark many of the major oceanic plate boundaries (Fig. 2). Undoubtedly plate tectonics is more successful when applied to the oceans; the plate boundary zones of submarine transform faults and, to a lesser extent, mid-ocean ridges are narrow.

Nonetheless, some oceanic deformation is poorly described by a model of rigid plates separated by narrow boundaries. For example, before 1985, India, Australia, and the intervening seafloor were treated as components of a single Indo-Australian plate (Fig. 3A), despite the occurrence of large earthquakes within the equatorial region of the Indian Ocean, far from the presumed plate boundaries (Figs. 1, 2, and 4) (*20, 21*). The seismic-moment release rate of these large earthquakes exceeds that along the San Andreas Fault in southern California (*21*). Reflection seismic profiles of the thick sediments in the Bengal Fan overlying equatorial Indian Ocean seafloor also show that this region has deformed (*22*). Instead of being flat-lying, as would be expected for deposition atop a rigid plate, the sediments are folded into wavelike undulations and are cut by high-angle reverse faults. The orientation of the folds and faults indicate that the oceanic crust is being shortened in a north-south direction. Undulations in the satellite-derived gravity field above the Indian Ocean also suggest north-south shortening (*23*). Moreover, plate motion data for the Indian Ocean are poorly fit if a single, rigid Indo-Australian plate is assumed (*16*).

At least two interpretations of this deformation are possible. One is to label it as intraplate deformation of the Indo-Australian plate. The other is to treat it as a wide boundary zone between distinct Indian and Australian plates (Fig. 3B) (*24–27*). The former view fails to predict the kinematics, whereas the latter allows the application of plate tectonics to predict the sense and sum of the deformation across the plate boundary zone. Because these predictions are success-

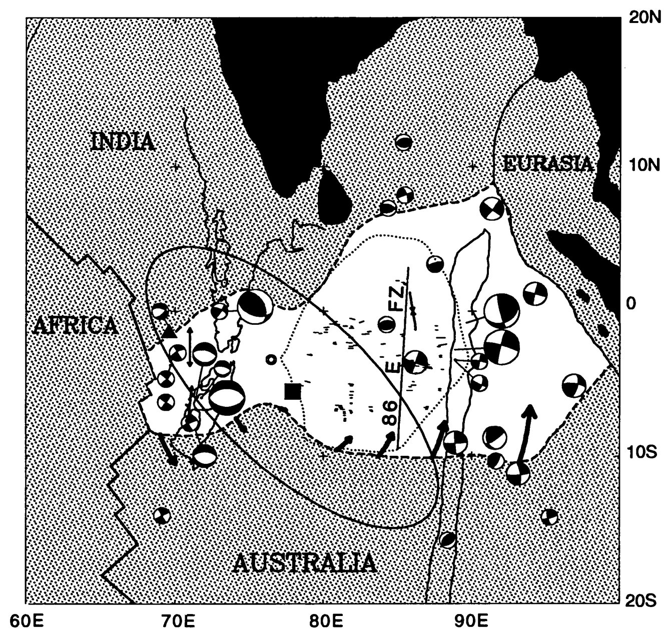

Fig. 4. Tectonic map of, and predicted motion across, the India-Australia plate boundary zone. A wide plate boundary zone (white area) separates the assumed-rigid Australian and Indian plates. The Australian plate moves counterclockwise relative to the Indian plate about an Euler pole (solid square), which has a 95% confidence region shown by the surrounding ellipse. The thick arrows on the Australian plate's northern border show the motion of the Australian plate relative to an arbitrarily fixed Indian plate. Thin lines within the diffuse boundary are faults with significant basement offsets. Dotted line shows approximate limits of area with east-west lineated gravity anomalies seen in Seasat data. Focal-mechanism symbol size increases with surface-wave magnitude (M_s). The large, intermediate, and small focal-mechanism symbols show the locations of earthquakes with M_s exceeding 7.0, between 6.0 and 7.0, and less than 6.0, respectively. Thin arrows show two average *T* axes for nine focal mechanisms near the Central Indian Ridge and an average *P* axis for four mechanisms near the Ninetyeast ridge. Published with the permission of the American Geophysical Union, from (*26*).

ful (Fig. 4), we conclude that the wide plate boundary zone model is more useful than the intraplate deformation model.

Wide plate boundary zones occur within oceanic lithosphere in several regions. The Gorda deformation zone takes up part of the motion between the Juan de Fuca and Pacific plates (*28, 29*) and can be interpreted as a wide plate boundary zone (*29, 30*). Another region where it seems likely that the deformation of oceanic lithosphere has been distributed is in the Atlantic west of the Mid-Atlantic Ridge and east of the Lesser Antilles. Morgan (*2*) recognized that North America may move relative to South America but could not resolve the motion with the sparse data then available. Later plate motion studies show that such motion is resolvable (*14–16, 31*), but only place broad limits on the location of any proposed boundary (*32*). Despite geophysical surveys and the monitoring of earthquakes for decades, no narrow boundary has been found, suggesting that the boundary is wide. Other examples of likely wide oceanic plate boundary zones are the lithosphere immediately west of the Macquarie Ridge Complex (*25, 33*), lithosphere east of the South Sandwich trench (*14*), the boundary between the Caroline and Pacific plates (*34*), and the western boundary between the Scotia and Antarctic plates (*35*).

The contrast of the narrowness of oceanic plate boundary zones with the great width of continental plate boundary zones has often been attributed to the differences in rheology. Given that it now appears that some oceanic plate boundary zones have widths similar to some continental plate boundary zones, the role of rheology in controlling the widths of oceanic plate boundary zones needs to be reexamined.

Another exception to the assumption of narrow boundaries occurs in the leading edge of the overriding plate at obliquely converging trench plate boundaries. Many plates overriding trenches include strike-slip faults that are typically 100 to 300 km distant from, and parallel to, the trench (*36, 37*). Examples include the Samangko fault (Sumatra), the Philippine fault, the Median Tectonic line (southwest Japan), the Atacama fault (Chile), the Dolores-Guayaquil fault (Colombia and Ecuador), and the Liquina-Ofqui fault (south Chile). Where such strike-slip motion occurs, the slip directions of the thrust earthquakes should not parallel the direction of motion between the underthrust plate and the interior of the overriding plate. If all the trench-parallel motion were taken up along the strike-slip fault or faults, then the slip directions in the thrust earthquakes would be perpendicular to the trench. Observed slip directions lie between the direction of plate motion and the perpendicular to the trench (*14, 37*). Moreover, the direction of motion estimated from earthquake slip directions along trench plate boundaries differs significantly in every case from independent estimates of the motion calculated from plate circuit closure (*14*). Thus, the slip directions are biased indicators (up to $\sim 30°$) of the plate motion direction and the trench-parallel motion is only partly taken up by strike-slip faulting. Trench-parallel motion of the forearc relative to the main overriding plate varies along strike and therefore is not simply the motion of a rigid forearc plate relative to the main plate (*38*). The thrust-faulting slip directions thus lend further support to the conclusion that part of the plate motion is taken up within the overriding plate. Diffuse seismicity in the leading edge of the overriding plate in many regions (*39*) also supports this interpretation.

Thus, plate tectonics, which satisfactorily describes the kinematics of much of Earth's surface, does not usefully describe the kinematics of many active deformation zones. These deformation zones seem more usefully described as wide plate boundary zones than as intraplate deformation zones. An ideal, comprehensive, physical model would predict when and where plates should be rigid and when and where plate boundary zones should be narrow or wide. Progress toward this goal requires an accurate description of the kinematics of wide plate boundary zones. Such a description requires measurement of motions across and within wide zones of deformation, as is now possible using space geodesy.

Space Geodesy

Space geodesy is a term applied to three techniques for making precise position measurements between sites on Earth's surface, which may be separated by as much as $\sim 12{,}000$ km. The three techniques, very long baseline radio interferometry (VLBI), satellite laser ranging (SLR), and the global positioning system (GPS), are based on technologies developed for space-related research, in particular radio astronomy and satellite tracking.

VLBI depends on the precise timing of radio noise from compact extragalactic sources observed at several radio telescopes. Analysis of the noise permits estimation of the location of a radio telescope site in the nearly inertial reference frame defined by the sources. In a typical geodetic VLBI experiment, two to seven radio telescopes simultaneously record noise from one source at a time and eventually record noise from 5 to 15 sources (*40, 41*). The noise recorded at different sites is correlated to determine delays and delay rates between telescopes. These data are used to determine site locations, the orientation of Earth, and azimuths to radio sources. Uncertainty in tropospheric delay and Earth orientation are the main cause of site location errors. Repeat experiments allow site motion to be estimated.

SLR is based on the round-trip time of laser pulses reflected off a satellite, such as the Laser Geodynamics Satellite (LAGEOS), which orbits at an altitude of about 5900 km. The distance or range to the satellite is one-half of the product of the speed of light and the elapsed time between emission of a laser pulse and its reception at the same tracking site. Range estimates from many sites determine both the satellite trajectory and the three-dimensional coordinates of the tracking stations. Successive observations permit the position of the tracking station to be estimated as a function of time (*42, 43*). Because the satellite orbit moves with Earth's center of mass (the geocenter), site motions are referred to a dynamically defined nearly inertial reference frame that moves with the geocenter.

GPS geodesy uses a constellation of high-altitude (20,000 km) satellites with orbital periods of 12 hours (*44, 45*). Each satellite broadcasts a message giving the time and an estimate of the satellite's position. The distance between the satellite and a GPS receiver can be estimated from the transit time of the message from the satellite to the receiver. When multiple satellites are simultaneously tracked, the location of the receiver can be estimated to within a few meters by trilateration. More sophisticated analysis techniques exploit the fact that the error sources (mainly uncertainties in satellite orbits, satellite and receiver clocks, and atmospheric radio delays) are common to a network of stations tracking the same satellites, and thus give relative positions repeatable to a few centimeters or less (*44*). The resulting positions are precise enough that changes between them can show tectonic motions within a few years. Like SLR, GPS locates sites in a dynamically defined, nearly inertial reference frame that moves with the geocenter.

The different space geodetic techniques have been used in complementary ways. Initially, VLBI and SLR were used for both global and continental scale studies, and for smaller scale regional experiments. As GPS technology has matured, it is being used more for regional studies owing to lower cost and smaller size of GPS receivers. These costs are becoming low enough that the long-term installation of a GPS receiver at a site will become common; GPS receivers are already permanently installed at several sites in southern California. In years to come most baselines likely will be measured with GPS, with VLBI and SLR providing sparser, longer distance measurements (46).

Space geodetic data already have made important contributions to tectonics. First, they have been used to test and verify the hypothesis that plate motions are steady, that is, that the rates and directions of plate motion averaged over a few years (the shortest interval over which meaningful rates can be obtained) are similar to rates and directions averaged over millions of years (the shortest interval over which rates have been estimated systematically from marine magnetic anomalies) (40, 43, 47–50) (Figs. 5 and 6). Second, space geodetic data have been used to estimate rates and directions of motion between plates or microplates for which no useful estimate was available from conventional plate motion data or conventional geodetic data (51, 52). This work has shown that the amount of motion between the Pacific and North American plates not taken up by strike-slip along the San Andreas fault in southern central California or by deformation farther east within the Basin and Range province is small and statistically unresolvable (52). Third, space geodetic data have been used to estimate the motion of individual small blocks within a plate boundary zone relative to a plate, albeit with gross undersampling of sites from a tectonic point of view (Fig. 7) (43, 45, 49, 53–56). Fourth, space geodetic data have been used to estimate rotations about a vertical axis of crustal blocks (57, 58). Fifth, space geodetic data have been used to resurvey monuments that were previously surveyed with conventional geodetic techniques to estimate deformation rates (59).

The first four contributions listed above come from two capabilities of space geodesy that are unavailable from earlier geodetic techniques. The first capability is the accurate measurement of the distance between sites that are beyond the line-of-site limitations of conventional geodesy. For example, estimates from VLBI of the motion between the Pacific and North American plates use sites in the Marshall and Hawaiian islands, Alaska, California, Texas, Colorado, Massachusetts, and Florida (47, 49).

The second capability is that site motion can be referred to a terrestrial reference frame defined by the motion of distant sites. From a conventional geodetic survey in a deforming zone, the rate of deformation between sites but not the rotation of sites about a vertical axis are estimated. Although the rotation could, in principle, be determined in conventional surveys using astronomic azimuths (60), block rotations have not been measured successfully by this means. A rigid-body rotation could be added to any set of velocities for the sites without affecting the fit to the observations (61). Space geodesy permits the motions of

Fig. 5. Rates from SLR (satellite-laser ranging) over about 10 years are compared with rates predicted by the NUVEL-1 global plate motion model (14), which was determined from transform fault azimuths, earthquake slip directions, and 3-million-year average spreading rates from magnetic anomalies over mid-ocean ridges. The rates of shortening or lengthening are along 54 great circles that cross at least one plate boundary and connect two sites in one of five plate interiors. The slope of the line is 0.949 ± 0.019, suggesting that the rates averaged over a decade may be a few percent slower than those averaged over millions of years, well within systematic errors and biases and the expected variation in plate velocities over millions of years. Published with the permission of the American Geophysical Union [after (43)].

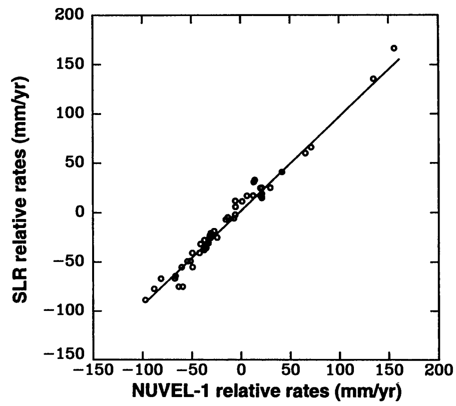

sites to be calculated relative to a set of sites that on geologic and geodetic grounds are believed to form a useful terrestrial reference frame. Such a set of sites can be taken to be those within the stable interior of a plate (62).

The ability to estimate rotations about a vertical axis is important in tectonics. Rotations between rigid plates can be inferred from conventional plate motion data. In the case of small oceanic plates and hypothesized nearly rigid continental microplates, the inferred rotation rate can be rapid (63, 64). Paleomagnetic studies have found surprisingly large rotations, up to 90° or more, within wide continental plate boundary zones (65). Accurate rotation rates can be determined from paleomagnetic data only if a block has rotated at a constant angular rate since the paleomagnetic samples were formed and if their age is known well. How such estimates of rates, which necessarily reflect averages over long intervals and which may come from rocks formed long before the rotation commenced, can be related to current motions and tectonics is not always clear. Rotation can be estimated from space geodetic data from the difference in velocity of two or more sites relative to a reference frame fixed with respect to a stable plate interior.

Steadiness of Plate Motion

Space geodetic data show that plate velocities averaged over a few years are similar to velocities averaged over millions of years (40, 43, 47–50, 66) (Figs. 5 and 6). In particular, the velocity between the Pacific and North American plates estimated from several years of VLBI data nearly equals the estimate from global plate motion model NUVEL-1 from spreading rates, transform azimuths, and earthquake slip directions (40, 47, 50). Both the VLBI data and NUVEL-1 give estimates of the relative velocity between the Pacific and North American plates that are ~8 mm/year slow-

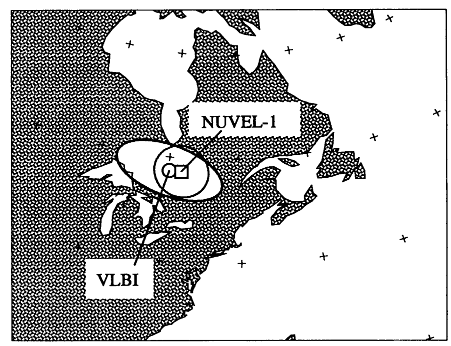

Fig. 6. Comparison of angular velocity vectors and their 95% confidence limits describing the motion between the Pacific and North American plates from 1984 to 1987 and over the past million years. The estimate from 1984 to 1987 is determined from VLBI (very long baseline interferometry) geodetic data and has a rotation rate of 0.81 ± 0.07° per million years. The estimate over 3 million years is from the NUVEL-1 global plate motion model and has a rotation rate of 0.78 ± 0.02° per million years. (14). Figure courtesy of D. Argus [after (47)].

er than predicted by earlier models of geologically instantaneous plate motion. Velocities estimated from space geodetic data between other pairs of plates are also very similar to that predicted by NUVEL-1, but may differ by small but significant amounts. For example, space geodetic estimates of velocities between North America and Europe are several millimeters per year slower than predicted from NUVEL-1 (43, 56). Changes in plate velocities of this size or larger are common over time scales of millions of years.

The observed steadiness of the motion of plate interiors may seem surprising in light of the episodic motion associated with earthquakes at plate boundaries. However, steadiness is an expected consequence of the dynamic equilibrium of driving forces (buoyancy forces and pressure gradients) with resistive forces in a highly damped convective system. Inertial forces are negligible in convection of the solid Earth, as shown by the miniscule Reynolds number of $\sim10^{-20}$ for whole-mantle convection. Consequently, episodic motions at plate boundaries are damped by the viscous asthenosphere to sum to the observed steady motion (67). Thus, geologists and geophysicists believe that plate motion rates estimated from marine magnetic anomalies, which average over millions of years, should be close to averages over much shorter intervals: tens of millennia, millennia, centuries, decades, years, or less. Plate velocities can change over long intervals of perhaps a million years or longer because of the gradual reconfiguration of plate boundaries or the arrival at a deep sea trench of anomalously buoyant crust. However, changes on a human time scale of years or decades are unexpected.

The working hypothesis of steady rates of plate motion permeates much research in which rates averaged over disparate lengths of time are compared and combined. In particular, estimates of geologically instantaneous plate motion combine data that average motion over decades with data that average motion over millions of years. The hypothesis of steadiness has been tested implicitly many times, for example, in models of global plate motion, and appears to be correct, as long as the tests are constructed so that the results are unaffected by elastic strain accumulated between earthquakes in plate boundary zones. The width of the zone of elastic strain accumulation has been measured in few regions, but for a strike-slip fault it is likely to be a few tens of kilometers, which is the width of elastic strain accumulation across the San Andreas fault in California where it is a single fault strand (61). Elastic strain may accumulate over a wider zone of a few hundred kilometers on the leading edge of the overriding plate at a subduction zone, as suggested by geodetic data from Japan (68).

The confirmation from space geodetic data of the similarity of plate velocities averaged over years to those averaged over millions of years extends the observed steadiness to an even shorter time scale. Possibly the most important implication is that one can combine rates averaged over intervals as long as millions of years with rates averaged over intervals as short as a few years when constructing models of the kinematics and tectonics of deforming zones of the crust and lithosphere (47).

Present and Impending Applications of Space Geodesy to Tectonics

Many important applications follow in the same directions as the recent research discussed above; these include (i) increasingly accurate estimation of plate motion averaged over years and testing for the steadiness of plate motion over even shorter intervals, (ii) densification of measurement networks within deforming zones to estimate the deformation and rotation rates, and (iii) estimation of plate motion that cannot be estimated reliably (or at all) from conventional plate motion data.

Plate convergence rates have been inferred only indirectly from conventional plate motion data because rate data are available only where plates diverge at a mid-ocean ridge. Space geodetic data can be used to construct strong independent tests of these predictions. The quantification of the partitioning of deformation across plate boundary zones, including how oblique convergence is distributed across a subducting or collisional plate boundary, is important. Many observations show that part of the oblique convergence at subducting plate boundaries is taken up in the leading edge of the overriding plate. Space geodetic observations from sites on both sides of the deforming region of an overriding plate would provide an integral constraint on the total deformation, although that motion does not determine the motion within the deforming zone uniquely (69–71). A denser network across the deforming region would provide even more information, which would complement other observations. For example, earthquake focal mechanisms give information on orientations of maximum shortening and lengthening, and in many cases the direction of slip, but do not describe the present deformation completely. Rotations relative to a distant external reference frame cannot be obtained from focal mechanisms. Moreover, slip rates are difficult to estimate accurately, both because of the uncertainties in time-averaged seismic slip estimates and because some of the slip may be aseismic. Using earthquake mechanism data together with a denser network of space geodetic data should help resolve these ambiguities.

Evidence for trench-perpendicular shortening in an overriding plate includes, for example, the existence of the Andean mountain belt and thrust faulting at its flanks. Global plate motion model NUVEL-1, which was determined from conventional plate motion data (14), predicts that the Nazca plate moves toward the stable interior of the South American plate east of the Andes at 83 mm/year. Unfortunately, this result tells us nothing about how much motion is taken up by subduction of the Nazca plate beneath South America, how much is taken up by shortening between the Pacific Coast and the stable interior of South America, or how that shortening is distributed. However, results from SLR indicate that a site at Arequipa (Peru), which lies in the western Andes, is moving 13 mm/year toward N76°E relative to the stable interior of South America (43), which suggests that ~15% of Nazca–South America plate motion is taken up by shortening within the Andes. Thus, the shortening seems rapid enough that a few years of space geodetic observations from a network of sites both east and west of the Andes zone could

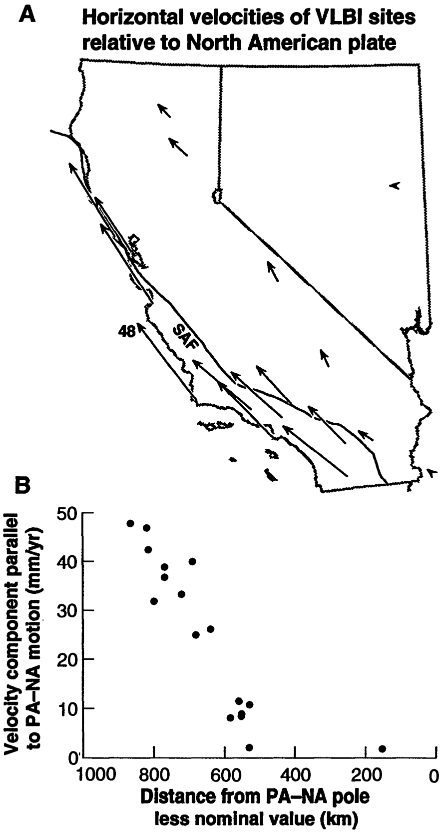

Fig. 7. (**A**) Horizontal vector velocities of VLBI sites in California, Nevada, and Arizona relative to stable North America. The velocity of the southwesternmost site nearly equals the 48-mm/year velocity of the Pacific plate relative to the North American plate. (**B**) Component of motion tangent to small circles centered on the NUVEL-1 Pacific–North America Euler pole (at 49°N, 78°W) versus great circle distance from that pole. The velocity of western U.S. crustal blocks in most places increases monotonically with distance southwestward from the Euler pole. Although the figure suggests that the velocities increase smoothly with distance from the Euler pole, there is a large velocity discontinuity due to the ~35 mm/year of time-averaged slip across the San Andreas fault in central California (61). Much of the remaining ~13 mm/year (the 48-mm/year velocity between the Pacific and North American plates minus the 35-mm/year San Andreas slip rate) is probably taken up in a shear zone a few tens of kilometers wide in the eastern Mojave desert and along the eastern edge of the southern Sierra Nevada (83). Figure courtesy of D. Argus [from (56); also see similar figure in (49)].

provide useful information on the distributed deformation.

Unlike the Nazca–South America converging plate boundary, the overriding plate at most convergent plate boundaries does not shorten but extends perpendicular to the trench (*72*). In some back-arc basins the rate of extension can be estimated from magnetic anomalies over a back-arc spreading ridge. However, back-arc extension may not be restricted to a single ridge, many back-arc basins lack interpretable anomalies, and most back-arc spreading ridges lack transform faults that can be used to estimate the direction of motion. Hence the motion of the leading edge of the overriding plate relative to either the main part of the overriding plate or the underthrust plate is known poorly, as is the subduction rate. Space geodesy can make an important contribution by quantifying these rates and directions of motion (*73*).

Estimates of the motion of the Sierra Nevada–Great Valley microplate relative to the Pacific and North American plates (*52*) illustrate another type of application of space geodesy, estimating the motion of rigid plates that cannot be related to other plates from conventional plate motion data. Nearly three-fourths [~35 mm/year (*74*)] of the 48 mm/year of motion between the Pacific and North American plates (*14*) is taken up by strike slip along the San Andreas fault in southern central California, which, along with the California Coast ranges, separates the Pacific plate from the Sierra Nevada–Great Valley microplate. The inferred angular velocity of the microplate relative to the North American plate (taken up by deformation in the Great Basin) (*75*) predicts a velocity of the eastern edge of the Sierra Nevada relative to stable North America of 11 mm/year toward N36°W, which accounts for nearly one-fourth of the 48 mm/year velocity between the Pacific and North American plates. The velocity nearly parallels the boundary between the Sierra Nevada and the Great Basin, which implies that current motion in the Great Basin results in a rotational, noncoaxial deformation. The vector sum of strike slip along the San Andreas fault and motion of the Sierra Nevada–Great Valley microplate relative to stable North America differs little from the relative velocity between the Pacific and North American plates. The difference can be described at 36°N along the San Andreas fault by a residual velocity vector with components of 5 mm/year parallel to the fault and 2 mm/year perpendicular to the fault with 95% confidence intervals of 0 to 10 mm/year and −1 to +5 mm/year, respectively. Thus, motion taken up by western U.S. deformation other than strike slip along the San Andreas fault or deformation in the Great Basin is small (*52*). A similar approach could be applied to estimating the motion of other plates or microplates including Southeast Asia, Turkey, and the Tarim craton, which is embedded in the broad collision zone between India and Eurasia.

An important application, not yet practical with available space geodetic data, will be finding the limits to plate rigidity in regions lacking earthquakes or other evidence of deformation. Because motions considered to be small from a geodetic perspective have dramatic geologic effects when taken up as contraction or extension, detecting deformation of plate interiors by space-geodetic techniques at a level that is otherwise unresolvable will require high accuracies, better than 1 mm/year (*76*). The accuracy of conventional plate motion data approaches but does not reach this level. Gordon *et al.* (*77*) formulated a test of plate circuit closure and hence of plate rigidity using conventional plate motion data. Application of this test to all conventional plate motion data shows that most plate circuits are consistent with closure (*13, 14, 25, 78*). None of the nonclosures found amounted to more than a ~3 mm/year of inferred deformation. Many nonclosures seem explainable by deformation marked by earthquakes in small salients of plates, and the statistical significance of many nonclosures is marginal. The nonclosures are small enough that all might be due to systematic errors in the plate motion data. Thus it seems likely that the accuracy needed to obtain convincing estimates of strain in plate interiors is high.

The accuracy of space geodetic rates depends mainly on three factors: (i) the accuracy of an estimate of a site location or the distance between sites found from each individual geodetic experiment, (ii) how often a site or monument is re-occupied in successive experiments, and (iii) the length of time over which the successive experiments are carried out—the longer the interval, the higher the accuracy. The accuracy of individual distance measurements is improving with time as both equipment and methods of data analysis improve. The repeatability of the estimates of distance between telescope sites provides an estimate of the precision of VLBI of 5 mm + 2×10^{-9} L, where L is the distance between sites in millimeters (*66*). Thus, 1000-km baselines are repeatable to about ~7 mm and 5000-km baselines are repeatable to ~15 mm. This gives a lower bound on the uncertainty because systematic errors are poorly known and difficult to estimate. The history of measurements using GPS is much sparser than for VLBI, but most space geodetic observations in the future will be made with GPS. The precision of GPS measurements can be estimated from repeatability between successive multiday measurements, which suggest horizontal precisions of several millimeters plus one to two parts in 10^8; vertical uncertainties are two to three times as large (*44, 45*). Given these distance accuracies, measurements must be made for at least a decade to approach a 1-mm/year rate accuracy at the 95% confidence level. The required measurement interval could be much longer if systematic errors are large, but may be briefer if improvements in equipment and technique sufficiently reduce the errors in individual measurements.

Although plate stability tests are likely to require rate accuracies of 1 mm/year or better, many important geological problems can be investigated with accuracies better than required to measure plate motion or rapid deformation, but worse than 1 mm/year. For example, space geodetic data may be able to measure the deformation in regions of slow or suspected deformation, such as the possibly continuing extension across the Rio Grande Rift and in rotating, modestly deforming regions, such as Afar (*64*). Space geodetic measurements should help to measure the contraction perpendicular to the San Andreas fault in southern central California, which produces conspicuous geological effects including the uplift of the Coast Ranges, but probably sums to no more than ~5 mm/year (*52, 59*).

The largest contribution that space geodesy is likely to make in the coming decade is in resolving fundamental questions about how best to describe the motion in plate boundary zones and the relation of that motion to the surrounding rigid plates. A great success of plate tectonics has been in its statistically efficient description of the motion between the major plates. For example, in global plate motion model NUVEL-1, which describes the motion between 12 major plates, 1122 high-quality data are well described by 33 adjustable parameters (*14*). This result implies that a model of rigid plates separated by narrow boundaries is useful, even if it may not apply to a significant minority of Earth's surface. This success suggests that the same kinematic model of rigid plates could be applied to ever smaller crustal or lithospheric blocks or microplates. To the extent that nearly rigid blocks can be defined, which we think they can nearly everywhere, this multiple-microplate approach would be correct. However, the most important property of a theory is its usefulness. As the number of blocks increases and the size of the blocks decreases in some deforming zones, the number of parameters needed to specify the kinematics can quickly become too large to be useful. Although the approach of specifying the angular velocity of rigid blocks can be usefully applied in several regions (for example, to the motion of the Sierra Nevada–Great Valley microplate), the blocks may be too small and too numerous for this approach to be useful in other regions.

Such considerations have led to alternative continuum formulations of the kinematics and dynamics of continental plate boundary zones (*69, 79*). These formulations are motivated in part by the belief that the strongest part of continental crust lies not in the brittlely deforming upper crust but in the plastically deforming uppermost mantle and that the brittle upper crust may passively mimic the deeper continuous flow (*80*). Insofar as deformation is homogeneous in a plate boundary zone, the kinematics can be specified by a constant velocity gradient tensor. Unfortunately, regionally homogeneous deformation of a brittle upper crust divided by discrete faults can have identical average velocity gradient tensors for different internal arrangements of faults and different accompanying rotations (*71*). Moreover, the regionally averaged deformation is unlikely to be homogeneous in many plate boundary zones, so that more parameters will be needed to specify how the deformation varies. One eventual test of the merits of the multiple-microplate and continuum approaches will be to examine which approach describes the characteristics of deformation of a plate boundary zone more efficiently, that is, with the fewest number of adjustable parameters. Another test will be to examine the extent to which either approach generates insights into the forces and stresses driving the deformation.

Conclusions

Plate tectonics is very successful in describing the kinematics and tectonics of the 85% of Earth's surface covered by rigid plates and by narrow plate boundaries. Carefully defined plate interiors appear rigid to within a few millimeters per year and possibly to much less. However, plate tectonics fails to describe the 15% of Earth's surface covered with deforming lithosphere. Much attention has been paid to such zones of distributed deformation in the continents, but significant portions of the oceanic lithosphere also form wide deforming zones. These zones are more usefully thought of as wide plate boundary zones than as zones of intraplate deformation.

Comparison of space geodetic data with predictions of geologically instantaneous plate motion models shows that plate velocities averaged over a few years are similar to plate velocities averaged over millions of years. Space geodetic data will help to answer many important remaining questions about the kinematics and dynamics of wide plate boundary zones. In particular, these data should help to determine whether a continuum or a multiple-microplate model, or some combination of the two, more usefully describes the kinematics of plate boundary zones. These data should also help to estimate the rates of shortening across mountain belts, the rates of extension across back-arc basins, and the rates of convergence between subducting plates and the leading edge of overriding plates. They also should help to quantify the degree of heterogeneity of deformation in plate boundary zones. The resulting improved description of plate boundary zone kinematics should usefully constrain estimates of the forces driving observed motion and deformation including plate motions, mountain building, crustal block rotation, and earthquakes.

REFERENCES AND NOTES

1. J. T. Wilson, *Nature* **207**, 343 (1965); D. McKenzie and R. L. Parker, *ibid.* **216**, 1276 (1967); X. Le Pichon, *J. Geophys. Res.* **73**, 3661 (1968).
2. W. J. Morgan, *J. Geophys. Res.* **73**, 1959 (1968).
3. H. H. Hess, in *Petrologic Studies: A Volume in Honor of A. F. Buddington*, A. E. J. Engel, H. L. James, B. F. Leonard, Eds. (Geological Society of America, Boulder, CO, 1962), pp. 599–620; R. Dietz, *Nature* **190**, 854 (1961).
4. F. J. Vine and D. H. Matthews, *Nature* **199**, 947 (1963).
5. W. C. Pitman III and J. R. Heirtzler, *Science* **154**, 1164 (1966); F. J. Vine, *ibid.*, p. 1405.
6. Spreading and convergence rates are taken from (*14*).
7. P. J. Fox and D. G. Gallo, *Tectonophysics* **104**, 205 (1984).
8. R. C. Searle, *J. Geol. Soc. London* **143**, 743 (1986).
9. P. Molnar and P. Tapponnier, *Science* **189**, 419 (1975).
10. K. C. Macdonald, in *The Geology of North America*, vol. M, *The Western North Atlantic Region*, P. R. Vogt and B. E. Tucholke, Eds. (Geological Society of America, Boulder, CO, 1986), pp. 51–68; in *The Geology of North America*, vol. N, *The Eastern Pacific Ocean and Hawaii*, E. L. Winterer, D. M. Hussong, R. W. Decker, Eds. (Geological Society of America, Boulder, CO, 1989), pp. 93–110.
11. A. Cox, R. R. Doell, G. B. Dalrymple, *Science* **144**, 1537 (1964); I. McDougall and F. H. Chamalaun, *Nature* **212**, 1415 (1966).
12. A. Baksi, B. Houghton, M. McWilliams, H. Tanaka, G. Turner, *Eos* **72**, 135 (1991).
13. D. F. Argus, R. G. Gordon, C. DeMets, S. Stein, *J. Geophys. Res.* **94**, 5585 (1989).
14. C. DeMets, R. G. Gordon, D. F., Argus, S. Stein, *Geophys. J. Int.* **101**, 425 (1990).
15. C. G. Chase, *Geophys. J. R. Astron. Soc.* **29**, 117 (1972); J. B. Minster, T. H. Jordan, P. Molnar, E. Haines, *ibid.* **36**, 541 (1974); C. G. Chase, *Earth Planet. Sci. Lett.* **37**, 355 (1978).
16. J. B. Minster and T. H. Jordan, *J. Geophys. Res.* **83**, 5331 (1978).
17. J. F. Dewey, and J. M. Bird, *ibid.* **75**, 2625 (1970); P. Molnar and D. Gray, *Geology.* **7**, 58 (1979).
18. W. F. Brace and D. L. Kohlstedt, *J. Geophys. Res.* **85**, 6248 (1980); S. H. Kirby, *ibid.*, p. 6353.
19. See, for example, P. Molnar, *Nature* **335**, 131 (1988).
20. B. Gutenberg and C. F. Richter, *Seismicity of the Earth and Associated Phenomena* (Princeton Univ. Press, Princeton, NJ, ed. 2, 1954); C. W. Stover, *J. Geophys. Res.* **71**, 2575 (1966); L. R. Sykes, *ibid.* **75**, 5041 (1970); S. Stein, *Geophys. J. R. Astron. Soc.* **55**, 577 (1978); D. A. Wiens and S. Stein, *J. Geophys. Res.* **89**, 11442 (1984).
21. S. Stein and E. A. Okal, *J. Geophys. Res.* **83**, 2233 (1978).
22. J. R. Curray and D. G. Moore, *Geol. Soc. Am. Bull.* **82**, 563 (1971); S. Eittreim and J. Ewing, *J. Geophys. Res.* **77**, 6413 (1972); J. K. Weissel, R. N. Anderson, C. A. Geller, *Nature* **287**, 284 (1980); C. A. Geller, J. K. Weissel, R. N. Anderson, *J. Geophys. Res.* **88**, 1018 (1983); J. R. Curray and T. Munasinghe, *Earth Planet. Sci. Lett.* **94**, 71 (1989); J. M. Bull, *Tectonophysics* **184**, 213 (1990) ——— and R. A. Scrutton, *Nature* **344**, 855 (1990); N. Chamot-Rooke *et al.*, *Eos* **72** (suppl.), 488 (1991).
23. D. C. McAdoo and D. T. Sandwell, *J. Geophys. Res.* **90**, 8563 (1985); W. F. Haxby, *Map* (National Oceanographic and Atmospheric Administration, Boulder, CO, 1987); C. A. Stein, S. Cloetingh, M. Wortel, *Geophys. Res. Lett.* **16**, 823 (1989); *Proc. Ocean Drilling Prog.* **116**, 261 (1990).
24. D. A. Wiens *et al.*, *Geophys. Res. Lett.* **12**, 429 (1985).
25. C. DeMets, R. G. Gordon, D. F. Argus, *J. Geophys. Res.* **93**, 11,877 (1988).
26. R. G. Gordon, C. DeMets, D. F. Argus, *Tectonics* **9**, 409 (1990).
27. J.-Y. Royer and T. Chang, *J. Geophys. Res.* **96**, 11,779 (1991).
28. E. A. Silver, *Geol. Soc. Am. Bull.* **82**, 2965 (1971); D. S. Wilson, *J. Geophys. Res.* **94**, 3065 (1989); P. R. Stoddard, *ibid.* **92**, 11524 (1987); *Tectonophysics* **187**, 205 (1991).
29. D. S. Wilson, *J. Geophys. Res.* **91**, 10259 (1986).
30. R. G. Gordon, *Rev. Geophys. Suppl.* **29**, 748 (1991).
31. S. Stein and R. G. Gordon, *Earth Planet. Sci. Lett.* **69**, 401 (1984).
32. D. F. Argus, thesis, Northwestern University (1990).
33. J.-Y. Royer and D. T. Sandwell, *J. Geophys. Res.* **94**, 13755 (1989); K. M. Marks and J. M. Stock, Eos **72** (suppl.), 444 (1991).
34. J. K. Weissel and R. N. Anderson, *Earth Planet. Sci. Lett.* **41**, 143 (1978).
35. A. M. Pelayo and D. A. Wiens, *J. Geophys. Res.* **94**, 7293 (1989).
36. T. J. Fitch, *ibid.* **77**, 4432 (1972).
37. R. D. Jarrard, *Rev. Geophys.* **24**, 217 (1986).
38. R. McCaffrey, *Geology* **19**, 881 (1991).
39. S. Stein, J. F. Engeln, D. A. Wiens, K. Fujita, R. C. Speed, *J. Geophys. Res.* **87**, 8642 (1982); G. Ekstrom and E. R. Engdahl, *ibid.* **94**, 15499 (1989).
40. T. A. Clark *et al.*, *ibid.* **92**, 12741 (1987).
41. J. W. Ryan *et al.*, *ibid.* **91**, 1935 (1986); P. M. Kroger, G. A. Lyzenga, K. S. Wallace, J. M. Davidson, *ibid.* **92**, 14,151 (1987); also see a recent review paper by J. R. Ray, *Rev. Geophys.* **29** (suppl.), 148 (1991).
42. S. C. Cohen and D. E. Smith, *J. Geophys. Res.* **90**, 9217 (1985).
43. D. E. Smith *et al.*, *ibid.* **95**, 22,013 (1990).
44. T. H. Dixon, *Rev. Geophys.* **29**, 249 (1991).
45. B. H. Hager, R. W. King, M. H. Murray, *Annu. Rev. Earth Planet. Sci.* **19**, 351 (1991).
46. Summaries of some of the many current GPS measurement programs are given in (*44 and 45*).
47. D. F. Argus and R. G. Gordon, *J. Geophys. Res.* **95**, 17,315 (1990).
48. C. G. A. Harrison and N. B. Douglas, *Tectonics* **9**, 935 (1990).
49. S. N. Ward, *J. Geophys. Res.* **95**, 21,9651 (1990).
50. T. Dixon *et al.*, *Geophys. Res. Lett.* **18**, 861 (1991).
51. J. B. Minster and T. H. Jordan, *J. Geophys. Res.* **92**, 4798 (1987).
52. D. F. Argus and R. G. Gordon, *Geology* **19**, 1085 (1991).
53. S. N. Ward, *J. Geophys. Res.* **93**, 7716 (1988).
54. C. Ma *et al.*, *ibid.* **95**, 21,991 (1990).
55. J Kellogg and T. H Dixon, *Geophys. Res. Lett.* **17**, 195 (1990); J. T. Freymueller and J. N. Kellogg, *Eos* **72**, 115 (1991).
56. D. F. Argus and R. G. Gordon, in preparation.
57. J. Jackson and P. Molnar, *J. Geophys. Res.* **95**, 22,073 (1990).
58. However, there are ambiguities due to the sparse-

ness of sites and the probable location of one of the sites in a zone of elastic strain accumulation.
59. K. L. Feigl, R. W. King, T. H. Jordan, *J. Geophys. Res.* **95**, 2679 (1990).
60. For example, J. Savage, *ibid.* **83**, 5487 (1978).
61. M. Lisowski, J. C. Savage, W. H. Prescott, *ibid.* **96**, 8369 (1991).
62. Such as in the tectonically stable portion of North America, that is, mainly east of the Rocky Mountains as in (*56*) also see (*49, 57*).
63. J. F. Engeln and S. Stein, *Earth Planet. Sci. Lett.* **68**, 259 (1984); J. F. Engeln, S. Stein, J. Werner, R. Gordon, *J. Geophys. Res.* **93**, 2839 (1988); R. C. Searle *et al.*, *Nature* **341**, 701 (1989).
64. G. D. Acton, S. Stein, J. F. Engeln, *Tectonics* **10**, 501 (1991); P. Tapponnier, R. Armijo, I. Manighetti, V. Courtillot, *Geophys. Res. Lett.* **17**, 1 (1990).
65. For example, M. E. Beck, Jr., *Am. J. Sci.* **276**, 694 (1976); R. W. Simpson and A. Cox, *Geology* **5**, 585 (1977); B. P. Luyendyk, M. J. Kamerling, R. R. Terres, J. S. Hornafius, *J. Geophys. Res.* **90**, 12454 (1985).
66. D. S. Caprette, C. Ma, J. W. Ryan, *NASA Tech. Memo 100765* (1990).
67. W. M. Elsasser, in *The Application of Modern Physics to the Earth and Planetary Interiors*, S. K. Runcorn, Ed. (Wiley, New York, 1969), pp. 223–246.
68. K. Shimazaki, *Phys. Earth Planet. Inter.* **8**, 148 (1974).
69. D. McKenzie and J. Jackson, *Earth Planet. Sci. Lett.* **65**, 182 (1983).
70. J. B. Minster and T. H. Jordan, in *Tectonics and Sedimentation Along the California Margin*, J. K. Crouch and S. B. Bachman, Eds. (Pacific Section, Society of Economic Paleontologists and Mineralogists, Los Angeles, 1984), vol. 38, pp. 1–16.
71. J. Jackson and D. McKenzie, *Geophys. J. R. Astron. Soc.* **93**, 45 (1988).
72. See, for example, the following review paper: W. Hamilton, *Geol. Soc. Am. Bull.* **100**, 1503 (1988).
73. For example, M. Bevis *et al.*, *Eos* **72**, 115 (1991).
74. See, for example (*61*).
75. The angular velocity is described by a right-handed rotation of 0.61° per million years about 32°N, 128°W, as documented in (*52*).
76. T. H. Jordan and J. B. Minster, in *The Impact of VLBI on Astrophysics and Geophysics, International Astronomical Union Symposium No. 129*, M. J. Reid and J. M. Moran, Eds. (Kluwer Academic, Boston, 1988).
77. R. G. Gordon, S. Stein, C. DeMets, D. F. Argus, *Geophys. Res. Lett.* **14**, 587 (1987).
78. R. G. Gordon and C. DeMets, *J. Geophys. Res.* **94**, 5560 (1989).
79. P. Tapponnier and P. Molnar, *Nature* **294**, 319 (1976); P. Bird and K. Piper, *Phys. Earth Planet. Inter.* **21**, 158 (1980); P. C. England and D. P. McKenzie, *Geophys. J. R. Astron. Soc.* **70**, 295 (1982); J. P. Vilotte, M. Daignieres, R. Madariaga, *J. Geophys. Res.* **87**, 10,709 (1982).
80. P. Molnar, in *Earthquake Mechanics, Rock Deformation, and Transport Properties of Rocks: A Festscrift in Honor of W. F. Brace*, B. Evans and T.-F. Wong, Eds. (Academic Press, London, in press); W.-P. Chen and P. Molnar, *J.. Geophys. Res.* **88**, 4183–4214 (1983).
81. The plate boundaries are mainly from (*82*) with the addition of the Scotia plate (*35*) and with a few boundaries refined.
82. D. F. Argus and R. G. Gordon, *Geophys. Res. Lett.* **18**, 2038 (1991).
83. R. K. Dokka and C. J. Travis, *ibid.* **17**, 1323 (1990); J. C. Savage, M. Lisowski, W. H. Prescott, *ibid.*, p. 2113.
84. This research was supported by National Science Foundation grant OCE-8900090 and National Aeronautics and Space Administration grant NAG5-885. We thank S. Agar, B. Cameron, and two anonymous reviewers for rapid and helpful reviews. The outlines of the idealized narrow plate boundaries and of the wide plate boundary zones shown in Fig. 1 incorporate several improvements made by T. Shoberg, who also prepared both Figs. 1 and 2.

Measured Trends in Stratospheric Ozone

Richard Stolarski, Rumen Bojkov, Lane Bishop, Christos Zerefos, Johannes Staehelin, Joseph Zawodny

Recent findings, based on both ground-based and satellite measurements, have established that there has been an apparent downward trend in the total column amount of ozone over mid-latitude areas of the Northern Hemisphere in all seasons. Measurements of the altitude profile of the change in the ozone concentration have established that decreases are taking place in the lower stratosphere in the region of highest ozone concentration. Analysis of updated ozone records, through March of 1991, including 29 stations in the former Soviet Union, and analysis of independently calibrated satellite data records from the Total Ozone Mapping Spectrometer and Stratospheric Aerosol and Gas Experiment instruments confirm many of the findings originally derived from the Dobson record concerning northern mid-latitude changes in ozone. The data from many instruments now provide a fairly consistent picture of the change that has occurred in stratospheric ozone levels.

Ozone is continuously being produced in the stratosphere by solar ultraviolet radiation. Radiation at wavelengths less than 242 nm dissociates molecular oxygen into atoms that attach themselves to O_2 to form ozone. The destruction of ozone in the stratosphere is dominated by the catalytic reactions of the nitrogen, hydrogen, chlorine, and bromine oxides. The ozone concentration peaks in the stratosphere at an altitude of 20 to 25 km. The distribution of ozone is maintained by a balance between its production and loss and by the transport of ozone from regions of net production to those of net loss. The transport of ozone is driven by the variable wind fields of the stratosphere, which give rise to daily fluctuations, seasonal variations, and interannual variability in ozone amounts.

Starting in the early 1970s, predictions have been made that human activities will lead to a diminishing of the earth's protective ozone layer (*1*). The search for evidence of downward trends in the thickness of the ozone layer was inconclusive until the discovery of the Antarctic ozone hole in 1985 (*2*). Ozone decreases during the Antarctic spring are now well documented (*3*). Ozone decreases outside the Antarctic, at southern mid-latitudes, have been reported, as well as over the heavily populated northern mid-latitudes (*4*).

Assessments of the state of knowledge about ozone depletion have been published in various joint reports from the World Meteorological Organization and the United Nations Environment Program. In this paper, based on a chapter of the most recent report (*5*), we review the evidence for ozone depletion and analyze some of the updated records.

R. Stolarski is at the Goddard Space Flight Center, Greenbelt, MD, 20771. R. Bojkov is at the World Meteorological Organization, Geneva 20, Switzerland 1211. L. Bishop is at Allied Signal, Buffalo, NY 14210. C. Zerefos is at the University of Thessaloniki, Thessaloniki, Greece 54006. J. Staehelin is at the Laboratory for Atmospheric Physics, ETH, 8093 Zurich, Switzerland. J. Zawodny is at the Langley Research Center, Hampton, VA 23665.

Sources of Data

Ozone measurements can be divided into two important types: those that measure the total thickness of the ozone layer and those that measure the ozone concentration as a function of altitude. Historically, the most important instrument for the measurement of the total thickness of the ozone layer has been the Dobson spectrophotometer, designed in the 1920s and still in use today. The Dobson instrument, located on the ground, measures the solar radiation transmitted through the ozone layer at pairs of wavelengths near 300 nm. One wavelength is chosen so that it is significantly absorbed by ozone while the other is attenuated in the instrument by a calibrated optical wedge. The wedge position is adjusted until equal signals for the two beams are obtained. Measurements are made for two separate pairs of wavelengths to allow cancellation of errors due to aerosols in the atmosphere (*6*).

Daily measurements have been made using a Dobson instrument at the station in Arosa, Switzerland, from 1926 to the present. Since 1957, a network of more than 30 stations has been making measurements of the total ozone thickness. This network is spread over much of the world but is heavily concentrated in the Northern Hemisphere (*7*). The network of instruments is calibrated relative to a single "world standard instrument," which is itself calibrated each summer at Mauna Loa. The calibration is then transferred to the rest of the instruments